Adventitial mast cell activation disrupts endothelial cell/pericyte interactions during early life allergic asthma

Régis Joulia[1*]#, Franz Puttur[1], Helen Stölting[1], Lewis J. Entwistle[1], Anna Voitovich[1], May Al-Sahaf[1,2], Katie Bonner[1,3], Elizabeth Scotney[1,3], Philip L Molyneaux[1,4], Richard J Hewitt[1,4], Simone A. Walker[1], Laura Yates[1], Sejal Saglani[1,3], Clare M. Lloyd[1]*#

[1] National Heart and Lung Institute (NHLI), Imperial College London, London, UK.

[2] Department of Thoracic Surgery, Hammersmith Hospital, London, UK.

[3] Department of Paediatric Respiratory Medicine, Royal Brompton Hospital, London, UK

[4] Royal Brompton and Harefield Hospitals, Guy's and St Thomas' NHS Foundation Trust, London, UK

Corresponding authors: r.joulia@imperial.ac.uk and c.lloyd@imperial.ac.uk

Summary

Allergic asthma generally starts during early life and is linked to significant tissue remodelling and lung dysfunction. Although angiogenesis is a feature of the disrupted airway, the impact of allergic asthma on the pulmonary microcirculation during early life is unknown. Here, using quantitative imaging in precision-cut lung slices (PCLS), we report that exposure of neonatal mice to house dust mite (HDM) extract disrupts endothelial cell/pericyte interactions in adventitial areas. Central to the blood vessel structure, the loss of pericyte coverage was driven by mast cell (MCs) proteases, such as tryptase, that can induce pericyte retraction and loss of the critical adhesion molecule N-Cadherin. Furthermore, spatial transcriptomics of paediatric asthmatic endobronchial biopsies revealed intense remodelling associated with increased expression of MC proteases in regions enriched in blood vessels. These data provide previously unappreciated insights into the pathophysiology of allergic asthma with potential long-term vascular defects.

Keywords: early life, lung, allergic asthma, vasculature, pericyte, mast cell, protease, imaging.

Introduction

Allergic asthma commonly develops during early childhood. While it is difficult to precisely define the prevalence of children affected it is now estimated that between 5% to 20% of all children are impacted by asthma (Dharmage et al., 2019; Mukherjee et al., 2016). Chronic Inflammation and tissue remodelling are central elements of allergic asthma. Although the immune mechanisms by which allergic responses are well characterised in adult pathologies (Hammad and Lambrecht, 2021; Lloyd and Saglani, 2019), our understanding of the impact of dysregulated immune responses in early life is only now being appreciated. In addition to airway hyperresponsiveness (AHR) and active tissue remodelling such as increased subepithelial basement membrane thickness, vascular remodelling is also a key feature of allergic asthma (Augusto et al., 2017; Harkness et al., 2015; Papi et al., 2018). Indeed, as the disease progresses, the newly altered tissue requires the formation of new blood vessels to efficiently irrigate the remodelled epithelium and adjacent areas (McDonald, 2001). The latter has been demonstrated in murine models and human biopsies where an increased number of blood vessels was observed in sub-epithelial areas (Salvato, 2001; Turato et al., 2008). Furthermore, most of the intermediate to large blood vessels present in the lungs are in close proximity to large epithelial areas described as bronchovascular spaces or adventitia which are involved in multiple pathologies such as asthma and helminth infections (Cautivo et al., 2022; Dahlgren et al., 2019; Stenmark et al., 2011; Turner et al., 2018). Central to the maintenance of blood vessels (Armulik et al., 2010; Attwell et al., 2016; Yuan et al., 2021), little is known about the interaction between endothelial cells and their associated mural cells, pericytes, during lung pathologies (Johnson et al., 2015; Rowley and Johnson, 2014; Yuan et al., 2021). Pericytes have a unique

ability to maintain endothelial cell fitness through the secretion of pro-angiogenic mediators but also cell-cell interaction involving adhesion molecules such as N-cadherin (Armulik et al., 2011).

Whilst lung function starts to decline in children with allergic asthma, the lung vasculature is still developing towards its adult form. Therefore, preventing remodelling during early-life is a critical window of opportunity to prevent disorders later in life. However, the mechanism by which the microcirculation and intermediate blood vessels in close vicinity to large airways is impacted by the responses to allergens remains enigmatic. In this context, mast cells (MCs) are key players in orchestrating the development of allergic asthma through the release of preformed mediators (e.g. histamine, proteases) in response to IgE/antigen or neuropeptide mediated stimulation (Bradding and Arthur, 2016; Hammad and Lambrecht, 2021). However, the mechanism by which MCs can regulate vascular inflammation during early life allergic asthma remains to be determined.

Here we used our precision-cut lung slices (PCLS) approach, innovative image quantification, functional assays and spatial transcriptomics to study the lung vasculature in the context of early life allergic airway disease (AAD). Using high dimensional analyses, we discovered that neonatal mice exposed to allergen exhibit vascular remodelling during disease progression which is defined by a loss of pericyte coverage, reduced number of blood vessels and development of hypoxic areas. Mechanistically, we identified a population of adventitial connective tissue MCs (CTMCs) that were highly activated following allergen exposure. *In vitro*, mouse and human MC granules were able to induce pericyte retraction and reduction of N-cadherin expression. The latter was mediated through MC protease activity and specifically, in human MCs, by tryptase. Finally, spatial transcriptomic data of

endobronchial biopsies from children with asthma showed increased expression of MC proteases specifically in vessel-rich areas. Together, our data has revealed a new MC/pericyte axis critical in disruption of lung vascular function during early life asthma with potential long-term consequences.

Results

Development of a quantitative imaging platform to study lung vasculature in neonatal mice.

To determine the impact of early life allergic airways disease on the vasculature, we extended our PCLS approach (Puttur et al., 2019) to simultaneously analyse the different components of the vessel wall, namely: endothelial cells and pericytes. Pericytes are a heterogenous population of cells expressing different phenotypic markers between and within organs (Armulik et al., 2011; Hung et al., 2019). We explored the human lung cell atlas data set to identify the most reliable markers of lung pericytes (Schupp et al., 2021b). The genes for PDGFRβ and NG2 (*CSPG4*) were the most highly expressed in mouse and human pericytes, and we focussed on PDGFRβ due to its greater level of expression in lung pericytes (Fig. S1A-B). PCLS explants obtained from lungs of neonatal mice were stained for CD31 (endothelial cells), α-SMA (smooth muscle cells, SMCs) and PDGFRβ (pericytes) and showed a rich and complex network of blood vessels. Interestingly, pericytes were highly abundant in adventitial regions associated with larger blood vessels but were also present across the parenchyma (Fig. 1A, Video S1). High magnification images revealed intimate cellular interactions between endothelial cells and pericytes, with extensive protrusions emerging from the pericyte cell body and surrounding endothelial cells (Fig. 1B). In addition, PDGFRβ^{+} cells were also positive for NG2 confirming their pericyte phenotype (Fig. S1C). We next developed an integrative platform to analyse vascular changes using our PCLS system. This platform relies on the use of tile scan imaging to identify the different lung regions (i.e. pleura, bronchovascular space/adventitia and parenchyma) and high-resolution images to define 3D structure and spatial organisation of blood vessels. Using IMARIS

software, we processed the images through cell segmentation and volume analyses. Together, we extracted 6 different parameters of vascular inflammation in the lungs: i) endothelial cell coverage (i.e. volume of endothelial cells within the image), ii) vessel density, iii) pericyte number, iv) pericyte coverage (i.e. volume of pericytes surrounding endothelial cells), v) distance between endothelial cell and pericyte and vi) number of $CD45^+$ cells (Fig. 1C). Together these parameters provide an accurate representation of the lung vascular architecture and its impact on inflammation.

Next, we employed our platform to analyse the lung vasculature in neonatal mice exposed to HDM. Seven-day old BALB/c mice were exposed to intermittent HDM, and lung lobes were collected at different times during disease progression (i.e. postnatal "PN" day 21 and 28) and during the resolution phase after the end of the exposure (i.e. PN day 35 and 42, Fig. 1D-E). We next performed an unsupervised principal component analysis (PCA) combining the 6 vascular parameters extracted from our images in 2 regions of the lungs (i.e. adventitia and parenchyma). Adventitia regions were identified using structural parameters (i.e. presence of a large airway and intermediate/large blood vessel) and the associated microvasculature within a 150 μm radius from the large airway and large vessel was analysed. Parenchyma was defined using alveoli structures far from any large airway (Fig. 1A). The PCA revealed alterations to the vascular structure as early as 2 weeks following HDM exposure (PN day 21). These changes were further exaggerated by the end of the allergen exposure (PN day 28) and were mainly linked to a loss of blood vessels. Whilst some mice still exhibited the same vascular changes at PN day 32 during the resolution phase, most had recovered a vasculature comparable to that of age-matched controls at PN day 42 (Fig. 1F).

In summary, our data clearly indicate that HDM exposure induced vascular remodelling in early life mainly due to vascular loss. These changes are maintained during the resolution phase but slowly resolve with time.

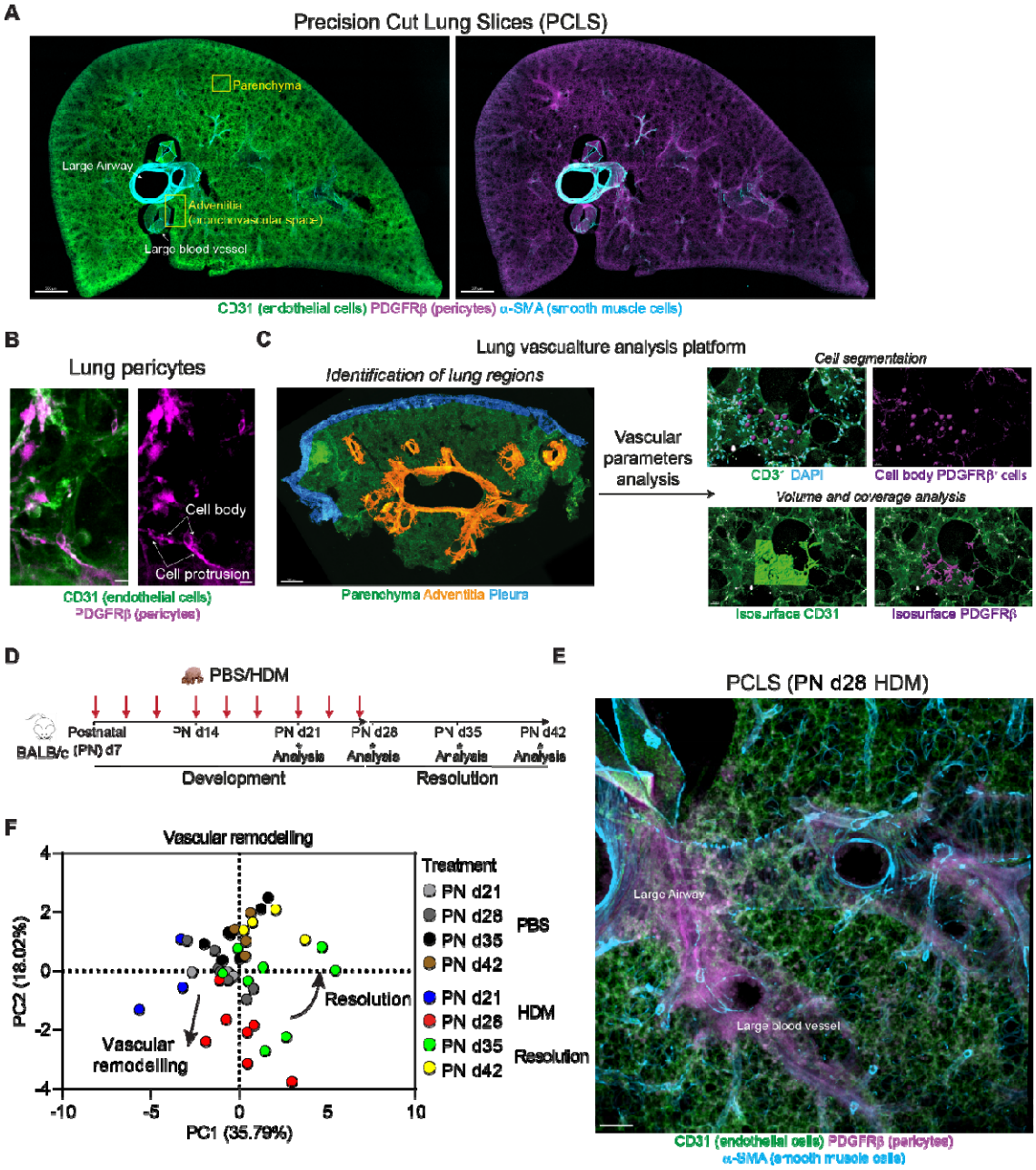

Figure 1: Allergen-induced inflammation leads to vascular remodelling in early life. (A) 3D rendering of a PCLS section (200 µm thickness) of neonatal lung (PN d28) stained for CD31 (green, endothelial cells), α-SMA (cyan, SMCs) and PDGFRβ (magenta, pericytes). Yellow box regions indicate adventitial and parenchyma regions analysed (see Video S1), scale bars 500 µm (representative of 4

independent experiments). (B) Zoomed in image of pericytes (PDGFRβ^{+}) extending protrusions around endothelial cells, scale bars 7 µm (representative of 4 independent experiments). (C) Image analysis pipeline showing the result of cell segmentation and volume analysis, scale bars 500 µm or 30 µm. (D) BALB/c mice aged 7 days were exposed to intermittent intranasal PBS or HDM for 3 weeks (red arrows). Lungs were collected at postnatal (PN) days 21, 28, 35 and 42. (E) PCLS section of HDM exposed neonates (PN d28) showing the vasculature in an adventitial region, scale bar 200 µm (representative of 4 independent experiments). (F) PCA analysis of lung vascular functions (see Sup S2), each dot represents a mouse from 4 independent experiments.

Loss of pericyte coverage occurs early in HDM exposed neonatal mice.

One of the principal parameters determining the vascular remodelling in our PCA analysis (Fig. 1F) was the change in pericyte coverage in close proximity to the lung adventitia. Pericyte coverage, or the volume of pericyte cell protrusions, is an essential factor to maintain endothelial cell fitness and overall blood vessel structure such as in the brain where they form the blood brain barrier (Armulik et al., 2010). During early life AAD, zoomed in images clearly indicate that whilst the endothelial cell structure was still present in close vicinity to large airways at PN d28, pericyte signal was greatly reduced (Fig. 2A & Video S2). Interestingly, our image analysis revealed that pericyte cell bodies were still present between PBS and HDM groups but the extent of pericyte protrusions was severely reduced following 3 weeks HDM exposure (Fig. 2A). Indeed, quantitative analysis confirmed that adventitial pericyte cell number was not significantly changed during mouse development or impacted by HDM exposure (Fig. 2B). In contrast, pericyte coverage was reduced after 3 weeks of allergen exposure (i.e. ~42% reduction) and slowly recovered in the resolution phase to nearly physiological levels 2 weeks post last HDM inhalation (Fig. 2C). We next analysed the extent of blood vessels reflected by the endothelial cell volume in our images, to assess the impact of this loss of pericyte protrusions (Fig. 2D). Interestingly, we found that whilst there was a small reduction in

endothelial cell volume at the end of the HDM exposure, this decrease was significant 1 week into the resolution phase (Fig. 2D-E). The latter may indicate that the reduction in pericyte coverage leads to a decrease in the microcirculation of lung adventitial regions (Fig. 2D-E). Finally, we assessed if the vascular changes would affect the local levels of oxygen in the tissue. To this end, we analysed the expression of hypoxia-inducible factor 1α (HIF-1α) in the vasculature (i.e. $CD31^+$ areas). Following 3 weeks of HDM exposure, the adventitial vasculature showed increased expression of HIF-1α, that was slowly recovered in the resolution phase (Fig. 2F-G). These data clearly indicate that allergen exposure during early life leads to hypoxic areas in the lung adventitia region that slowly resolve in time.

Collectively, these data demonstrate, for the first time, that repeated exposure to allergen during the early life developmental period induces loss of pulmonary pericyte protrusions and blood vessels leading to hypoxic areas in the pulmonary microcirculation.

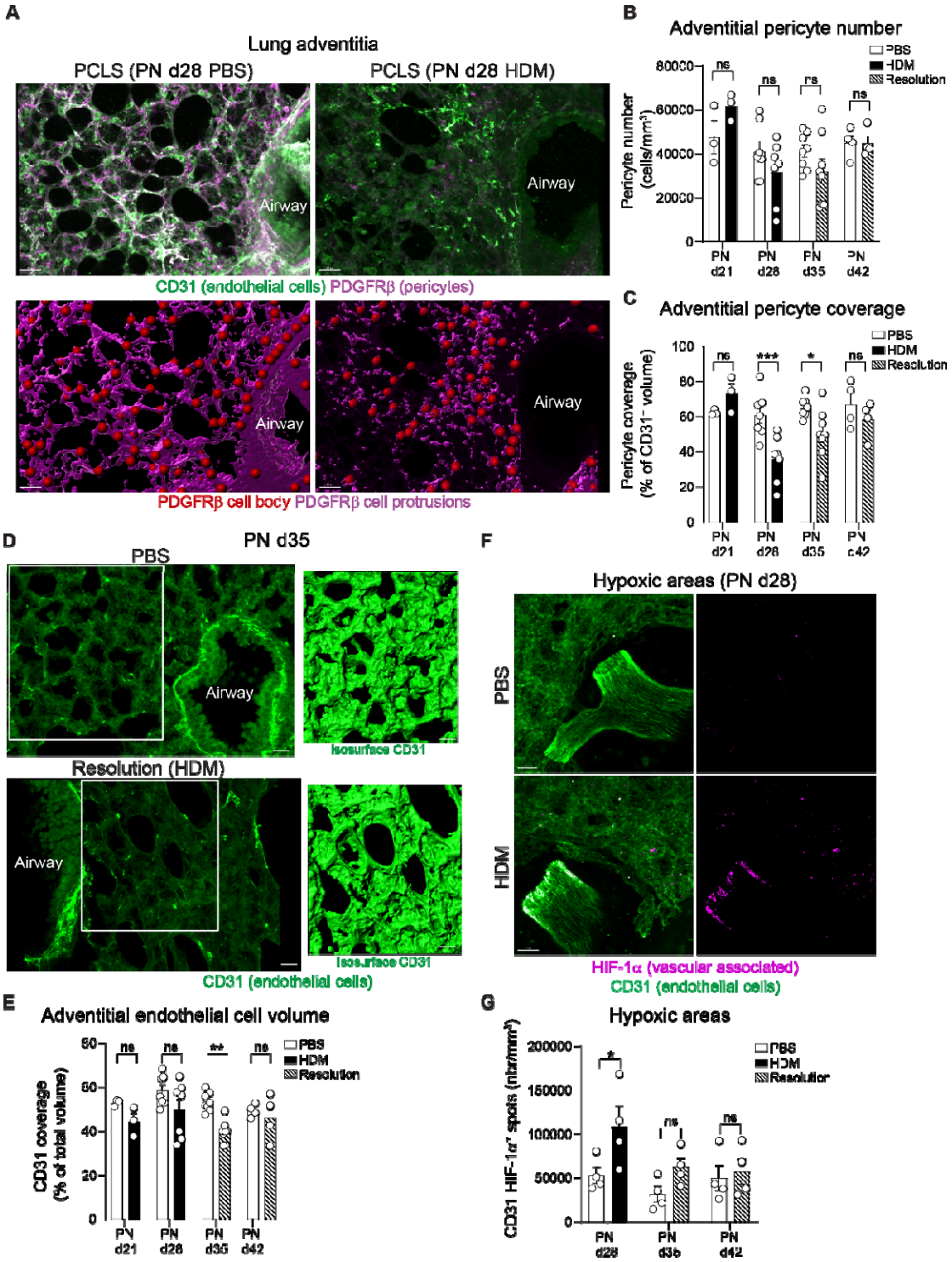

Figure 2: Repeated HDM exposure leads to loss of pericyte protrusions, reduced volume of blood vessels and hypoxic areas. Neonate mice were exposed with PBS or HDM as indicated in Fig. 1D. (A) 3D rendering of a PCLS section in PBS and HDM exposed mice 3 weeks post first inhalation showing CD31 (green, endothelial cells) and PDGFRβ (magenta, pericytes). Lower panels show the pericyte cell body (red dots) and protrusions (magenta surface) analysis (see Video

S2), scale bars 30 µm (representative of 4 independent experiments). (B-C) PDGFRβ$^+$ pericyte number per mm^3 (B) and coverage (C, normalised to the total volume of CD31$^+$ blood vessel) in the lung adventitia (n=3-8 mice per group from 4 independent experiments). (D) Representative PCLS showing a reduced microcirculation area 1 week into the resolution phase, scale bar 20 µm (representative of 4 independent experiments). (E) Adventitial endothelial cell coverage (normalised to the total volume of the image, n=3-8 mice per group from 4 independent experiments). (F) PCLS of HDM exposed mice for 3 weeks exhibiting increased HIF-1α (purple) associated to the vasculature (CD31, green), scale bars 30 µm (representative of 4 independent experiments). (G) Number of HIF-1α spots in adventitial region in PBS and HDM exposed mice (n= 4 mice per group). Mean ± SEM *p<0.05, **p<0.01,***p<0.001, ns=not significant.

Lung adventitia is marked by immune cell infiltration and mast cell activation

Lung adventitial regions are characterised by an abundant presence of resident immune cells coupled with intense recruitment of various leukocytes during inflammation (Cautivo et al., 2020; Dahlgren et al., 2019; Puttur et al., 2019). We hypothesized that local activation of the immune system may play a role in the vascular remodelling and changes in pericyte morphology observed in our neonatal mice following inhaled HDM exposure. Therefore, we employed our image analysis platform to dissect immune cell recruitment and activation following HDM exposure (Fig. 3A) in the lung adventitia (~150 µm from large airway/large blood vessel) and parenchyma. We observed a significant increase in the number of adventitial CD45$^+$ leukocytes following each HDM exposure (i.e. ~36% and ~40% increase after 2 and 3 weeks of HDM, respectively), with the difference still present 1 week into the resolution phase (i.e. ~60% increased), and returning to physiological levels 2 weeks following the end of the allergen exposure period (Fig. 3A-B). Irrespective of the inflammatory status, we demonstrated that ~50% of immune cells were found within 40 µm of an adventitial region within the lungs (Fig. 3A-C). Immune cell recruitment was mainly restricted to the adventitia since the lung parenchyma did not show a significant increase in leukocytes (Fig. S3A-B).

Given that MCs play a key role in allergic asthma, and we recently demonstrated the impact of perivascular connective tissue mast cells (CTMCs) in regulating pericyte function (Joulia et al., 2022), we hypothesized that MCs could play a role in mediating pericyte change during early life AAD. We utilised fluorescent avidin staining to analyse in detail the profile of degranulated CTMCs as we and others have demonstrated that it provides an accurate measurement of the localisation and cellular interactions of extracellular CTMC granules (Dudeck et al., 2019; Dudeck et al., 2021; Gaudenzio et al., 2016; Joulia et al., 2015). The number of CTMC did not change in HDM exposed neonatal mice as described in HDM exposed adult mice (Derakhshan et al., 2021; Xing et al., 2011) (Fig. S3C). However, we observed a clear increase in the number of degranulated CTMCs (Fig.3 D-E and Video S3). We found extracellular CTMC granules were abundant in the lung adventitia and within the parenchyma but not in the lung pleural cavity (Fig. 3F). These granules retain a large volume (i.e. ~50 μm^3) even outside of the MC cell body and no differences were observed between adventitial and parenchymal MC granule volume (Fig. 3G, Video S3). Interestingly, we observed a negative correlation between the volume of these granules and the reduction in pericyte coverage (r^2= 0.18, p value= 0.007, Fig. 3H) indicating that regions with large extracellular CTMC granules are associated with change in pericyte morphology. Furthermore, the presence of CTMC granules was linked with an increased distance between endothelial cells and pericytes (Fig. S3D).

In summary, our data show that upon exposure to allergens, neonatal mice develop strong adventitial inflammation linked with activation and degranulation of resident CTMCs. Areas with large CTMC granules are associated with destabilisation of endothelial cell/pericyte interaction that likely disrupt the vasculature.

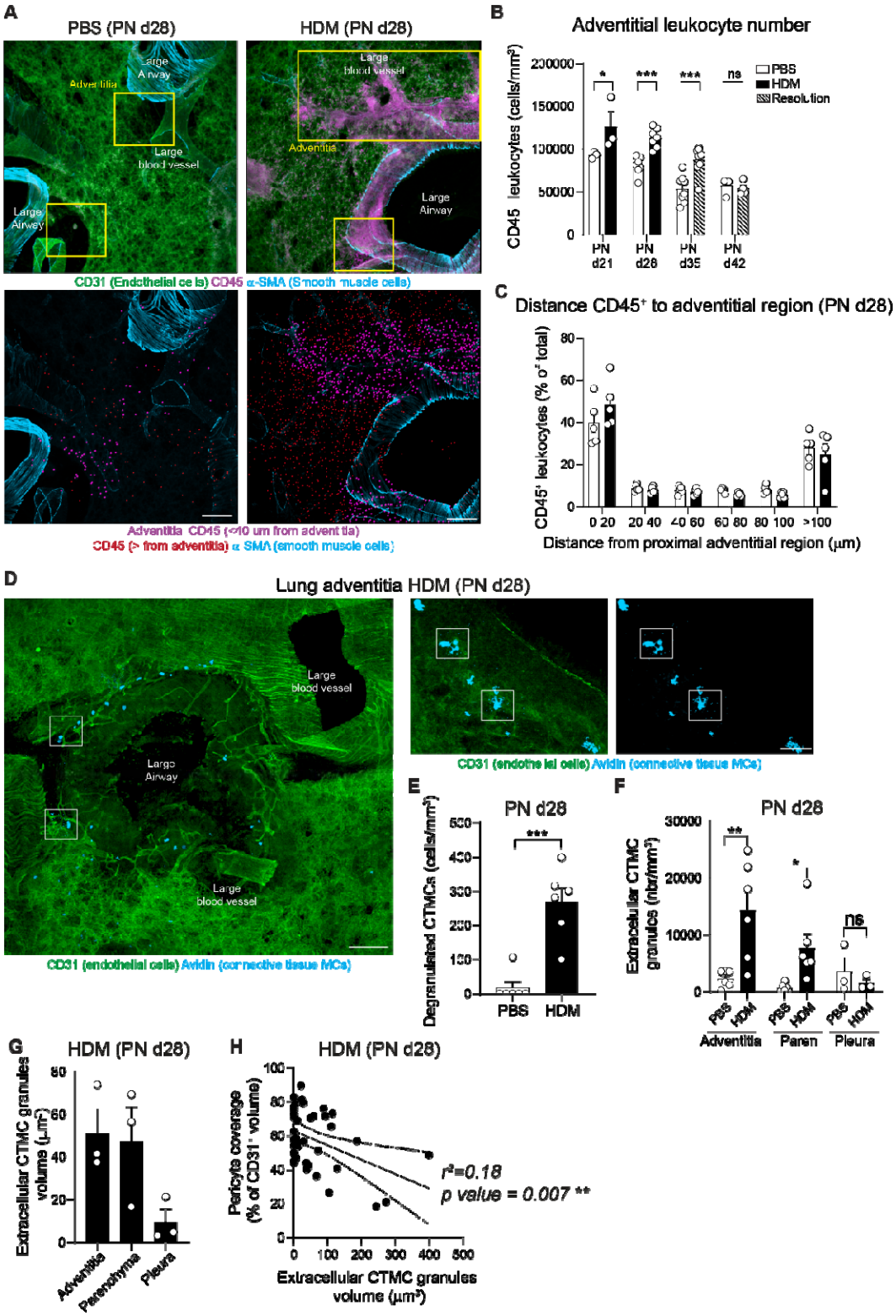

Figure 3: Early life allergen exposure leads to immune cell recruitment and MC activation in the lung adventitia. (A) 3D rendering of a PCLS in the lung adventitia in PBS and HDM exposed mice at PN 28 showing CD31 (green, endothelial cells), α-SMA (blue, SMCs) and CD45 (magenta, leukocytes). Lower panels show the CD45^{+}

cell body analysis, scale bars 200 µm (representative of 4 independent experiments). (B) $CD45^+$ cell number (n=3-8 mice per group from 4 independent experiments). (C) Distance between $CD45^+$ leukocytes and closest adventitial area (n=5 mice per group from 3 independent experiments). (D) Representative 3D image of lung adventitia showing the distribution of connective tissue MCs (avidin, blue) around a large airway and associated vasculature (CD31, green) and zoom-in images showing degranulated MCs adjacent to large airways and blood vessels (see Video S3), scale bars 150 µm and 50 µm (representative of 4 independent experiments). (E) Number of degranulated MCs (n= 6 mice per group). (F-G) Number of extracellular MC granules per mm^3 (F) and volume (G) (n=3-6 mice per group from 3 independent experiments). (H) Correlation between pericyte coverage and volume of extracellular MC granules (each dots represent an image analysed from n=5 mice). Mean ± SEM *p<0.05, **p<0.01,***p<0.001, ns=not significant.

CTMC degranulation induces pericyte retraction and loss of N-Cadherin

To analyse the functional impact of CTMC degranulation on lung pericytes, we developed an *in vitro* co-culture model between primary lung MCs and pericytes. Lung cells were purified from naïve mouse lungs and following 2-4 weeks in culture, a high level of purity was detected for both cell populations with expression of characteristic markers: $NG2^+/PDGFR\beta^+$ and $Fc\varepsilon RI^+/ST2^+/CD117^+$ for pericytes and MCs respectively (Fig. S4A). In addition, lung MCs were positive for avidin signal indicating that the *in vitro* generated MCs were indeed CTMCs (Fig. S4A). Anti-dinitrophenyl (DNP) IgE sensitized lung MCs were added to a layer of fluorescently labelled pericytes ($CMTMR^+$) and stimulated with increasing concentrations of DPN-BSA to induce FcεRI crosslinking and degranulation (Fig. 4A). Whilst the frequency of degranulated MCs increased proportionally with the concentration of DNP-BSA, the volume of pericytes decreased significantly 24h after stimulation (~30% reduction for 100 ng/ml DNP-BSA, Fig. 4B-D). We next investigated if the reduction in volume was more pronounced in pericytes that were directly in contact with MC granules. Avidin mean fluorescence intensity (MFI) on the largest pericytes (i.e. >45000 μm^3) showed lower avidin signal compared to the smallest pericytes (i.e. <17000 μm^3)

indicating that the smallest pericytes had more MC granules on their surface that could induce their retraction (Fig. 4E). Furthermore, one of the main consequences of pericyte retraction is the polarisation of F-actin (Kureli et al., 2020). Indeed, concomitant with reduced pericyte volume, the increased number of degranulated MCs led to an enhanced intracellular F-actin signal within pericytes (Fig. 4F-G). Interestingly, N-Cadherin expression, one of the main cadherins involved in the interaction between endothelial cells and pericytes (Procter et al., 2021) was decreased following contact with MC granules (~20% reduction at 100 ng/ml DNP-BSA, Fig. 4H).

Collectively, MC granules can efficiently induce pericyte retraction in a dose-dependent manner and facilitate reduction in N-Cadherin expression.

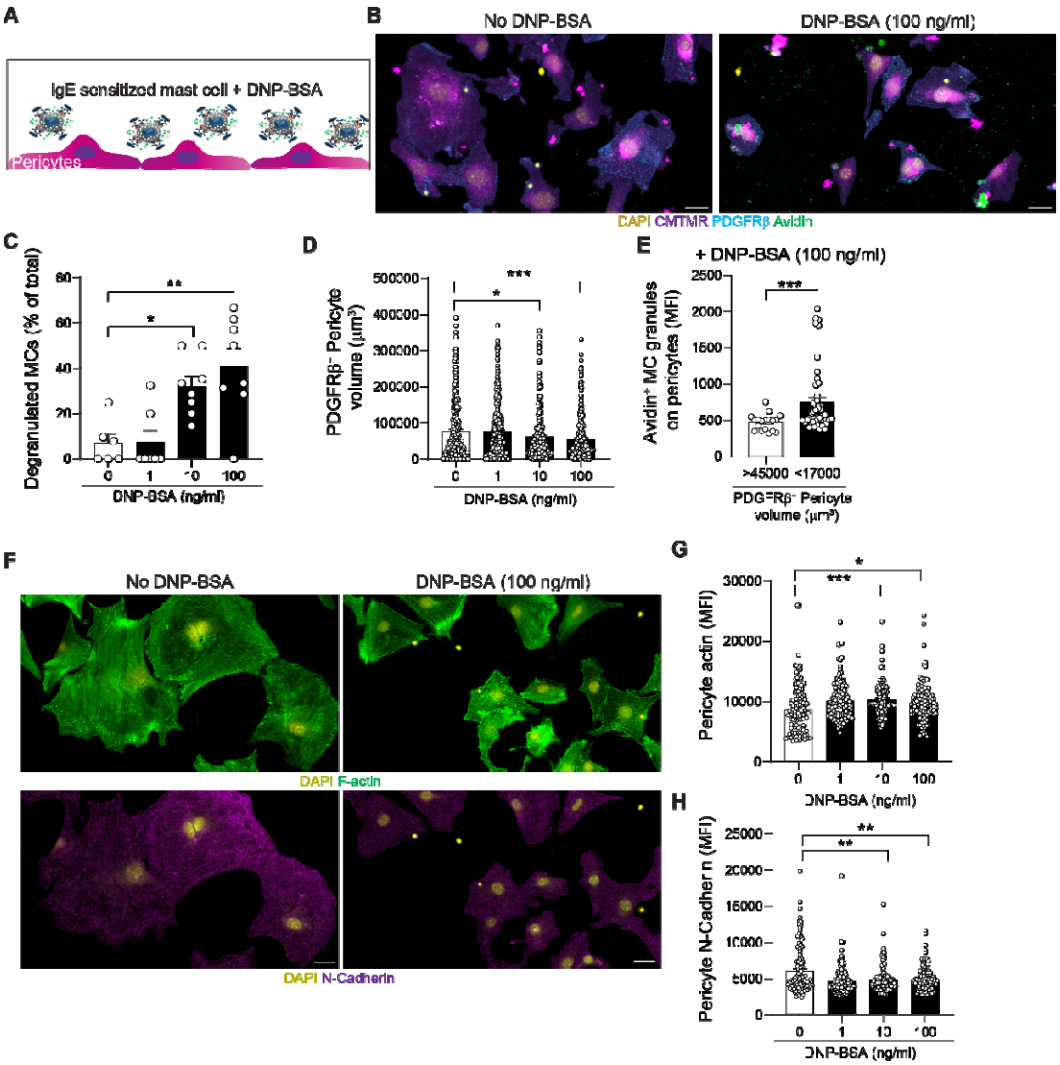

Figure 4: MC granules bind to pericytes and induce retraction and loss of N-cadherin. MCs were sensitized overnight with anti-DNP IgE then placed on a layer of pericytes (stained with CMTMR) and stimulated with increasing concentrations of DNP-BSA for 24 hours. (A) Schematic depicting the coculture experiment between primary mouse lung MCs and pericytes. (B) Images of unstimulated or stimulated (100 ng/ml DNP-BSA) pericyte/MC co-cultures stained for DAPI (yellow), CMTMR (purple), PDGFRβ (blue) and avidin (green, MC granules), scale bars 40 µm (representative of 3 independent experiments). (C) Number of degranulated MCs (normalised to the total number of MCs, each dot represents an image from 3 independent experiments). (D) Pericyte volume determined using the cell tracer CMTMR (each dot represents an individual pericyte from 3 independent experiments). (E) Avidin signal on small pericytes (<17000 µm^3) and large pericytes (>45000 µm^3) showing that small pericytes exhibit more MC granule staining on their surface (each dot represents an individual pericyte from 3 independent experiments). (F) Representative images of F-actin (green) and N-Cadherin (magenta) pericyte expression in the presence of degranulated MCs or control, scale bars 50 µm (representative of 3 independent experiments). (G-H) F-Actin (G) and surface N-Cadherin (H) MFI on pericytes (each dot represents an individual pericyte from 3

independent experiments). Mean ± SEM *p<0.05, **p<0.01,***p<0.001, ns=not significant.

Pericyte retraction and N-Cadherin loss are mediated by MC proteases

Having observed a reduced pericyte volume and N-Cadherin expression on pericytes following MC degranulation, we next investigated the molecular mechanisms of MC induced pericyte retraction. MCs contain a vast repertoire of proteases, which are involved in protective immunity against venoms and parasites but can also be detrimental in the context of inflammatory pathologies such as asthma (Pejler, 2019; Pejler et al., 2010). We hypothesized that MC derived proteases could be involved in pericyte retraction. Indeed, PCLS of HDM exposed neonates (PN d28) indicated that proteases such as m-MCP6 (MC tryptase) were present in CTMC granules (Fig. 5A). Furthermore, detailed colocalization analysis indicated the presence of m-MCP6 in extracellular MC granules, 24 hours post last HDM challenge, as demonstrated by their overlap with avidin^{+} regions (Fig. 5B-C). The latter agrees with the requirement for mMCP-6 to be associated with the CTMC granule matrix to be stored and activated efficiently (Pejler et al., 2010; Roy et al., 2016). We next tested if a general protease inhibitor could prevent pericyte loss of protrusions in the presence of degranulated MCs. Interestingly, our results showed that although MC degranulation was not impacted by the protease inhibitor (Fig. 5D-E), pericyte volume and N-Cadherin surface expression were maintained (Fig. 5F-G). To further confirm this observation, we directly exposed lung pericytes to recombinant m-MCP6 and observed a ~62% reduction in pericyte volume indicating that m-MCP6 at a high concentration is sufficient to induce pericyte retraction (Fig. 5H).

Together, these data demonstrate that MC proteases can efficiently induce pericyte retraction and loss of surface N-cadherin and potentially lead to loss of the endothelial cell/pericyte interaction.

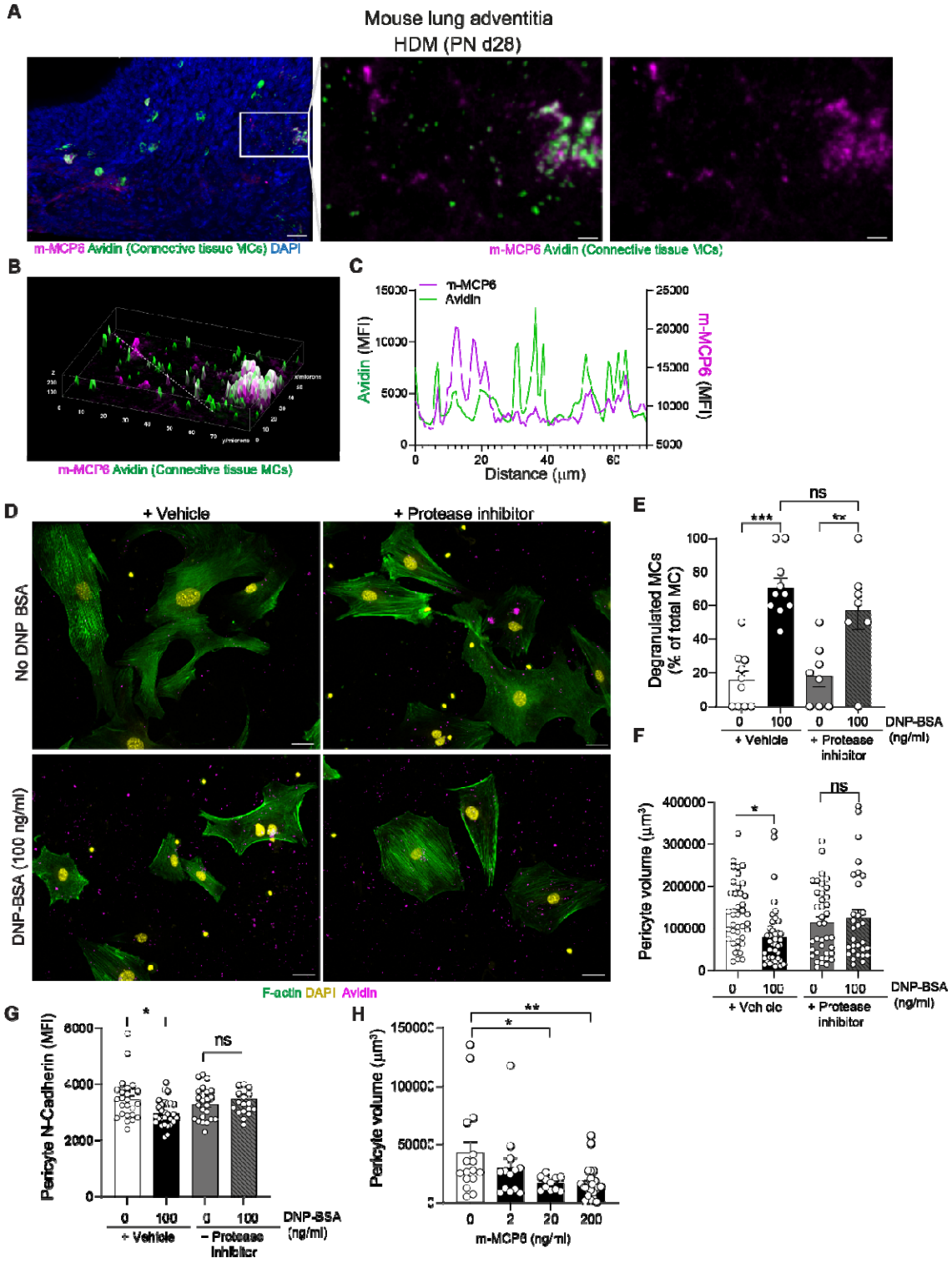

Figure 5: MC induced pericyte retraction and N-Cadherin loss is dependent on proteases. (A-B) Neonate mice were exposed to HDM as indicated in Fig. 1D and analysed at PN d28. (A) 3D rendering of a PCLS section in the lung adventitia in HDM exposed mice showing DAPI (blue), m-MCP6 (mouse tryptase, magenta) and

MCs (avidin, green), right panels show zoomed-in images of the white box region and the m-MCP6 signal in extracellular MC granules, scale bars 30 and 10 µm. (B) Colocalization analysis between MC granules (avidin) and m-MCP6, height of the peaks represents signal intensity. (C) Avidin and m-MCP6 immunofluorescence intensities along the dashed line in (B) showing presence of m-MCP6 in extracellular MC granules (representative of 3 independent experiments). (D-G) MCs were sensitized overnight with anti-DNP IgE then placed on a layer of pericytes (stained with CMTMR) and stimulated with increasing concentration of DNP-BSA for 24h in the presence of a protease inhibitor cocktail or vehicle control (DMSO). (D) Images of unstimulated or stimulated (100 ng/ml DNP-BSA) pericyte/MC co-cultures stained for DAPI (yellow), F-actin (green) and MC granules (avidin, magenta), scale bars 50 µm (representative of 3 independent experiments). (E) Number of degranulated MCs (normalised to the total number of MCs, each dot represents an image from 3 independent experiments). (F) Pericyte volume (each dot represents an individual pericytes from 3 independent experiments). (G) Surface N-Cadherin MFI on pericytes. (H) Lung pericyte volume 24h following recombinant m-MCP6 exposure (each dot represents an individual pericyte from 3 independent donors). Mean ± SEM *$p<0.05$, **$p<0.01$, ***$p<0.001$, ns=not significant.

Spatial transcriptomic analysis indicated signs of vascular remodelling and increased tryptase in children with asthma.

We next employed digital spatial profiling with the NanoString GeoMx® Cancer Transcriptome Atlas (CTA, ~1,800 genes) to analyse vascular remodelling and MC activation in children with severe asthma (between 9 and 17 years old, Table S1). Formalin-fixed paraffin-embedded (FFPE) sections obtained from endobronchial biopsies were stained for DNA, Vimentin, CD45 and α-SMA to determine 4 types of regions namely: epithelium (defined using morphology and DNA stain), immune cell infiltrate ($CD45^+$ rich), smooth muscle, and vessel-rich areas (Fig. 6A). Vessel-rich areas were defined by the presence of a clear ring structure (i.e blood vessel) associated with $vimentin^+$ cells. UV-photocleavable barcode-conjugated RNA *in situ* probes were hybridized on tissue sections, and multiple regions of interest (ROIs) were defined per sample using fluorescence staining. Following cleavage and collecting of barcodes from each ROI, the abundance of barcodes was determined using sequencing (Zimmerman et al., 2022).

We analysed 33 ROIs and first defined the pathways differentially regulated in epithelium and vessel-rich areas using gene set enrichment analysis (GSEA). Integrin cell surface interaction, extracellular matrix (ECM) reorganisation, ECM proteoglycans and integrin cell surface interactions were the most enriched pathways in vessel-rich regions compared to the epithelium, indicating vascular areas in children are more prone to remodelling, a hallmark feature of asthma. In line with the presence of allergens and inflammation, pathways linked to cellular stress such as reactive oxygen sensing (ROS), cellular response to chemical stress and antiviral mechanisms were increased in the epithelium (Fig. 6B-C). Interestingly, the gene for tryptase (i.e. *TPSAB1*), one of the most abundant MC proteases, was upregulated in vessel-rich areas, prompting us to investigate if MC phenotype was altered in this region (Fig. 6C). We employed single cell RNA-seq cell-type signatures to perform cell deconvolution (Deprez et al., 2020). Overall, we detected significant MC signatures (i.e. 52 genes) in the 4 different lung regions (Fig. S5A). Interestingly, PCA analysis revealed considerable heterogeneity in MC phenotype at least in part driven by the location of the MCs within the tissue (Fig. 6D). Moreover, MCs from vessel-rich areas showed a mixed profile between $CD45^+$ rich areas and smooth muscle (Fig. 6D). We next analysed the differentially expressed genes (DEGs) in the MC signature from vessel-rich areas compared to $CD45^+$ and epithelium ROIs. Genes for proteases such as tryptase (*TPSAB1*) and carboxypeptidase (*CPA3*) and the FC fragment of the IgE receptor (*FCERIG*) were enriched in vessel-rich areas indicating an enhanced content of MC-specific proteases in these regions (Fig. 6E-F). Furthermore, spatial visualisation of tryptase expression *in situ* showed a clear high abundance of *TPSAB1* and *CPA3* in vessel-rich areas compared to other lung regions in children with asthma (Fig. 6G, Fig.

S5B). Next, we analysed endothelial cell and pericyte signatures using a similar cell deconvolution strategy (Deprez et al., 2020) (Fig S5C-D). Although we detected several clusters for both populations, they did not associate with any lung regions analysed (Fig. S5E-F). Finally, we analysed the spatial distribution of HIF-1α as an indicator of vascular stress and observed a high expression of the marker in $CD45^+$, vessel and epithelial rich areas suggesting local changes in O_2 level in these regions (Fig. S5I).

Taken together, our data demonstrated for the first time the presence of a specialised population of MCs in vessel-rich areas of the lungs with increased protease content that could impact the vasculature locally during childhood.

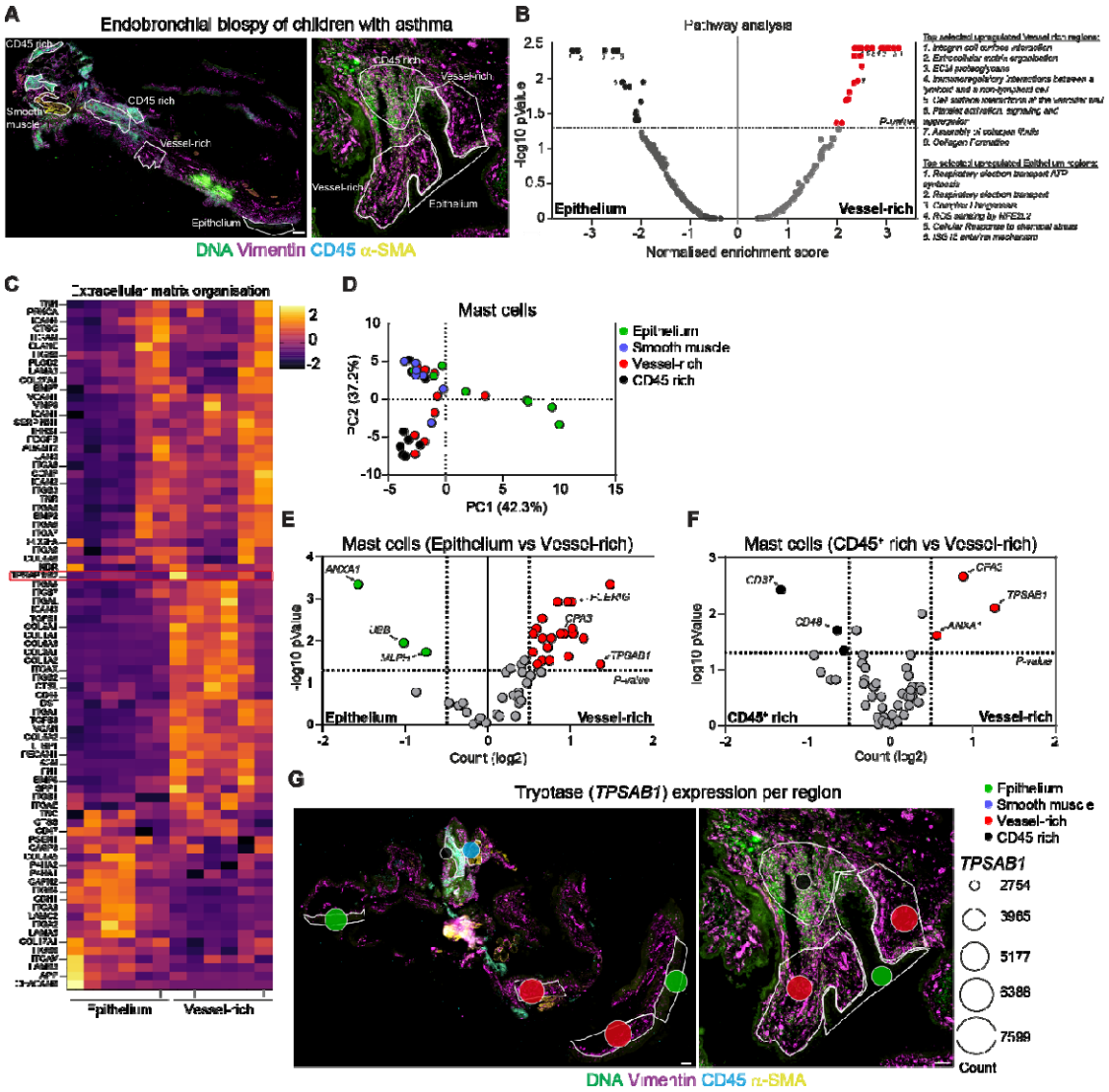

Figure 6: Increased remodelling and MC tryptase in vessel-rich areas of children with asthma. (A) Representative immunofluorescence images of endobronchial biopsies stained for DNA (Syto83, green), Vimentin (purple), CD45 (blue) and α-SMA (yellow) showing the selected ROIs (boxed regions), scale bars 100 µm (representative of the 3 children with asthma). (B) Volcano plot indicating the most upregulated pathways in epithelium versus vessel-rich areas); dotted line indicates the significance threshold (p value= 0.05). (C) Extracellular matrix organisation gene levels in epithelium and vessel-rich areas represented as a heat-map with a z-score colour code (n=6 representative ROIs per lung region). (D) PCA analysis of MC signature genes in the different ROIs identified. (E-F) Volcano plots exhibiting the differences between MC genes of CD45^{+} rich versus vessel-rich areas (E) and epithelium versus vessel-rich areas (F); dotted line on y axis indicates the significance threshold (p value= 0.05) and dotted line on x axis indicates the level of expression threshold (0.5 log2). (G) Spatial expression of TPSAB1 (tryptase) showing enriched expression in vessel-rich areas, dot diameters indicate the expression level.

Human lung pericytes retract following MC degranulation

Finally, we isolated human pericytes and MCs from healthy lung tissue and performed co-culture experiments. Isolation and culture methods yielded purities of more than 95% for both cell types (Fig. S4B). We exposed lung pericytes to IgE-sensitized MCs and increasing concentrations of DNP-BSA for 24h (Fig. 7A). Following MC degranulation, we showed a significant reduction in pericyte volume (Fig. 7B) and, as observed using murine cells (Fig. 4E), pericyte retraction was enhanced in cells in close contact with MC granules (Fig. 7C). To get a better insight into the molecular mechanism of MC dependent pericyte retraction, we analysed the content of extracellular MC granules by flow cytometry. Following 30 min IgE-mediated stimulation, we performed an unsupervised analysis (i.e. t-SNE) of membrane-bound MC granules (i.e. avidin^{+} MC (Joulia et al., 2015)) pooling 3 independent stimulated lung MC donors (Fig. 7D). We discovered strong heterogeneity in the profile of extracellular MC granules with the presence of cytokines such as IL-6 and TNF and an abundant presence of tryptase in ~63.7% of extracellular MC granules (Fig. 7D). Since tryptase is highly expressed in vessel-rich regions of the lung from children with asthma (Fig. 6E-G) and present in extracellular MC granules, we hypothesized that tryptase could directly induce pericyte retraction. Therefore, we performed co-culture experiments between activated MCs and pericytes in the presence of a specific tryptase inhibitor (i.e. APC-366) (He et al., 1998; Joulia et al., 2015). Whilst APC-366 did not impact MC degranulation (Fig. 7E-F), pericyte volume was maintained in the presence of the inhibitor (Fig. 7E and G).

Overall, MCs in human lungs are highly abundant and closely associated with blood vessels. Our data clearly indicate that tryptase released from human MCs induces

loss of pericyte protrusions and consequently destabilisation of blood vessel integrity.

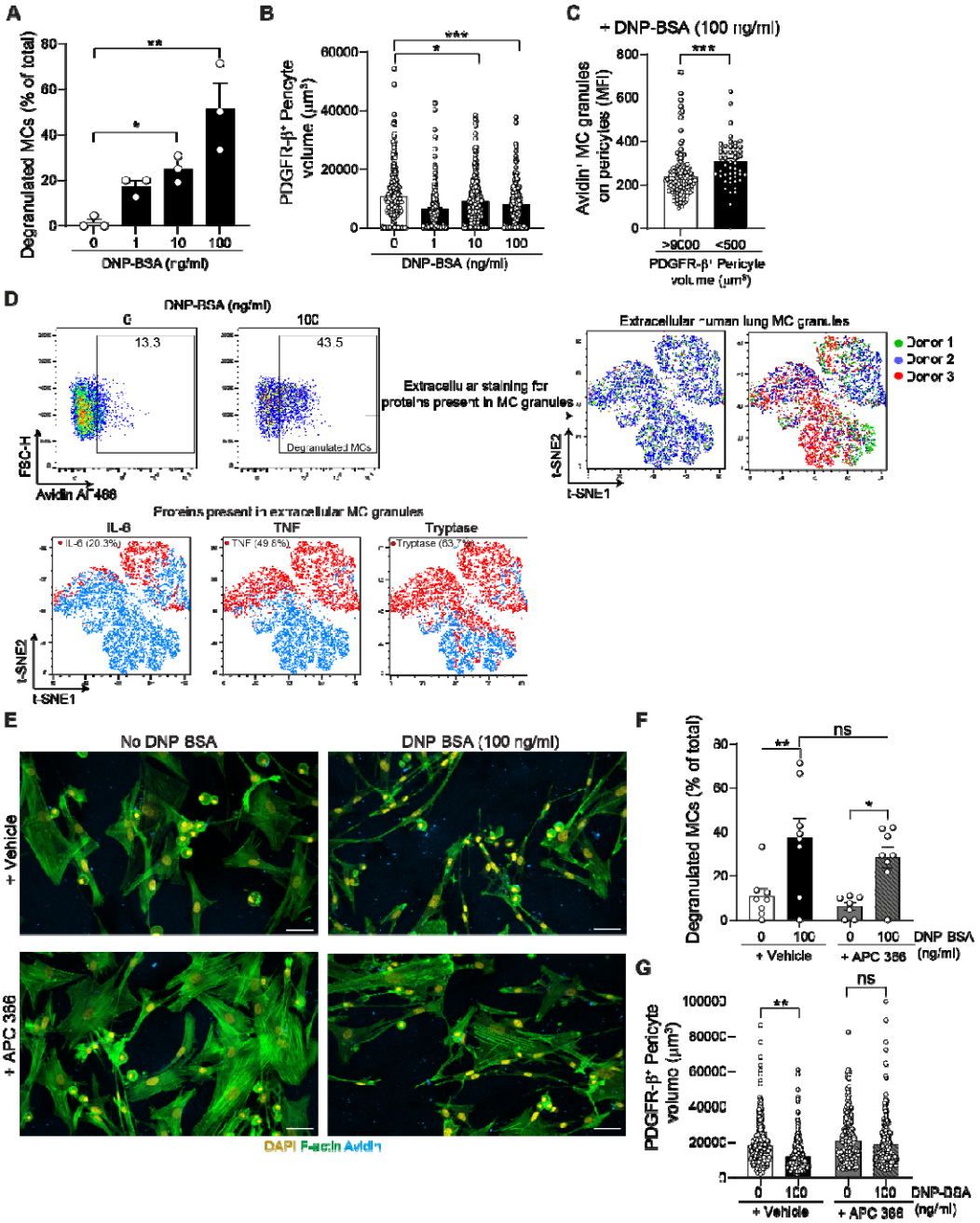

Figure 7: Human MCs induce tryptase dependant pericyte retraction. (A-C and E-G) Human MCs were sensitized overnight with anti-DNP IgE then placed on a layer of pericytes (stained with CMTMR) and stimulated with increasing concentration of DNP-BSA for 24h, in some experiments (C-E) APC366 (tryptase inhibitor) or vehicle control were added at the time of stimulation. (A) Number of degranulated MCs (normalised to the total number of MCs, each dot represents an

image from 3 independent experiments). (B) Pericyte volume (each dot represents an individual pericyte from 3 independent experiments). (C) Avidin signal on small pericytes (<500 μm^3) and large pericytes (>9000 μm^3) showing that small pericytes exhibit more MC granule staining on their surface (each dot represents an individual pericyte from 3 independent experiments). (D) Flow cytometry profiles of degranulated MCs and unsupervised analysis of extracellular MC granules, red dots indicate positive cells for the indicated markers (t-SNE analysis performed on 3 pooled donors, representative of 2 independent experiments). (E) Images of unstimulated or stimulated (100 ng/ml DNP-BSA) pericyte/MC co-culture stained for DAPI (yellow), F-actin (green) and MC granules (avidin, blue), scale bars 50 µm (representative of 3 independent experiments). (F) Number of degranulated MCs (normalised to the total number of MCs, each dot represents an image from 3 independent experiments). (G) Pericyte volume (each dot represents an individual pericyte from 3 independent experiments). Mean ± SEM *$p<0.05$, **$p<0.01$,***$p<0.001$, ns=not significant.

Discussion

Allergic airway diseases disproportionally impact children at a stage of their life when lungs are still developing structurally - including the vast vascular network. Despite our growing understanding of the distinctions between adult and neonatal immune responses (de Kleer et al., 2016; Saglani et al., 2018; Saluzzo et al., 2017), the impact of respiratory diseases such as allergic asthma on the lung vasculature remains elusive. Tissue remodelling such as increased thickness of the reticular basement membrane and collagen deposition is a key feature of chronic inflammation and angiogenesis is classically associated with this phenomenon (Papi et al., 2018; Saglani et al., 2018; Saglani et al., 2013). Indeed, as the tissue adjacent to the airway is expanding, newly developed bronchial blood vessels are required to supply the necessary nutrients. Paradoxically, how the original pulmonary microcirculation in adventitial regions adapt to the newly developed tissue currently remains unclear. Here, we demonstrate that pulmonary exposure to inhaled allergens such as HDM during early life drives important vascular changes in the lung adventitia and bronchovascular space. For the first time, we provide an accurate characterisation of the cascade of events leading to vascular remodelling starting with a reduction in pericyte coverage associated with a loss of blood vessels concomitant with increased hypoxic regions in specific lung regions. We show that the loss of protrusions from the pericyte surface are driven by proteases released following mast cell degranulation. Finally, spatial transcriptomic analysis indicated a strong remodelling signature in vessel-rich areas of lungs from children with asthma associated with increased protease content (i.e. tryptase and CPA3) that can induce human pericyte retraction.

Endothelial cell-pericyte interaction is an essential component of the stability of blood vessels however the mechanisms by which this interaction is dysregulated during inflammation remain poorly understood (Barkaway et al., 2022). Here, we identified that whilst the number of pericytes did not change dramatically throughout lung development or following exposure to allergens, the reduction in pericyte coverage was one of the earliest events observed for the vasculature during the development of AAD. The role of pericytes in lung biology is still poorly understood, fate mapping and depletion models provided the first evidence for the involvement of pericytes in lung pathologies such as pulmonary hypertension and lung fibrosis (Bordenave et al., 2020; Hung et al., 2022). Our data concur with previous work showing that in adult mice, the disruption of the PDGFβ-PDGFRβ axis worsened lung functions such as airway hyperreactivity (Johnson et al., 2015). The reduction in pericyte coverage is reminiscent of other pathologies such as Alzheimer's disease or following stroke. The latter drives a reduction in blood flow in specific areas leading to a decline in brain function (Nikolakopoulou et al., 2019; Nortley et al., 2019). Although our data indicate a loss of pericyte cell extension and increased hypoxic areas indicated by increased HIF1α expression, the impact of the latter on the blood flow in the lungs remains to be determined. Mechanistically, we show that mouse and human MC-derived granules induce pericyte retraction. Pericytes respond to a variety of inflammatory stimuli such as ROS, prostaglandin E2 and TNF (Barkaway et al., 2022) however, to our knowledge, the impact of MCs on pericyte coverage has never been described before. We identified that MC-derived proteases such as tryptase induce pericyte retraction and loss of N-Cadherin. The latter is a crucial junctional molecule mediating endothelial cell-pericyte interactions (Kruse et al., 2018) and further studies are required to understand how MC proteases can cleave

N-cadherin. In addition, the mechanism by which pericyte retraction occurs is still not fully elucidated, however recent evidence suggests a crucial role for F-actin and its associated regulators such as the Arp2/3 complex (Erdener Ş et al., 2022; Kureli et al., 2020).

Lung adventitial regions have recently received great interest and spatial analysis has started to uncover their specialised immune regulation (Cautivo et al., 2022; Dahlgren et al., 2019). In this context, we showed that lung adventitial regions were central to the inflammatory and remodelling response during early life AAD. Indeed, most of the vascular changes and inflammatory cell recruitment observed were confined to this region, confirming the essential role of spatial approaches to analyse lung immune responses. However, the identity of pericytes in these adventitial regions and whether there is a subclass of pericytes operating during development that are more susceptible to inflammation remains to be determined (Madissoon et al., 2022).

Interestingly, we identified a population of connective tissue MCs present around the airway and large blood vessels in neonatal developing lung. This agrees with previous studies which showed an increase in MC numbers from day 7 after birth (de Kleer et al., 2016). Our data extend this observation by determining the cellular location of MCs and explores their functional involvement during AAD. The specific distribution of MCs in these regions during early life remain unclear but the presence of specialised populations of cells such as adventitial stromal cells (ASCs) producing IL-33 (Dahlgren et al., 2019) could lead to the development of MCs (Allakhverdi et al., 2007). In addition, IL-33 is a potent MC activator able to regulate the extent of MC degranulation and production of chemokines (Joulia et al., 2017). However, despite evidence that IL-33 is critical for immune responses during early life

(Castanhinha et al., 2015; Saglani et al., 2013), the precise impact of IL-33-induced MC activation during early life remains to be explored. Interestingly, spatial transcriptomic analysis of endobronchial biopsies from children with asthma revealed, for the first time, distinct clusters of MCs highlighting a potential unreported diversity in human MC populations present during development. These differences highlight the importance of topographical information as to cell location during health and disease (Madissoon et al., 2022). Key open questions remain as to whether these clusters are driven by the immune response to allergens and if they are maintained during progression to adulthood. The association between MCs and blood vessels has been reported previously (Cheng et al., 2013; Choi et al., 2018; Dudeck et al., 2021; Kunder et al., 2011) however our data clearly indicate a specific profile of MCs adjacent to blood vessels with increased protease content. In summary, our study demonstrates that tissue remodelling, induced by inhaled allergens, impacts blood vessel organisation during early life with a reduction of the pulmonary microcirculation that precedes other structural changes. This loss of blood vessels in specific areas may negatively impact gas exchange. Together, the need for increased oxygen supply due to tissue expansion and the concurrent reduction in pulmonary vasculature will lead to a quicker deterioration of lung and vascular function overall. Moreover, our study increases our fundamental understanding of temporal and regional responses during lung pathologies. Finally, we uncovered a new axis of regulation for tissue remodelling during allergic inflammation involving MCs and pericytes that require further exploration during respiratory disorders (Figure 8).

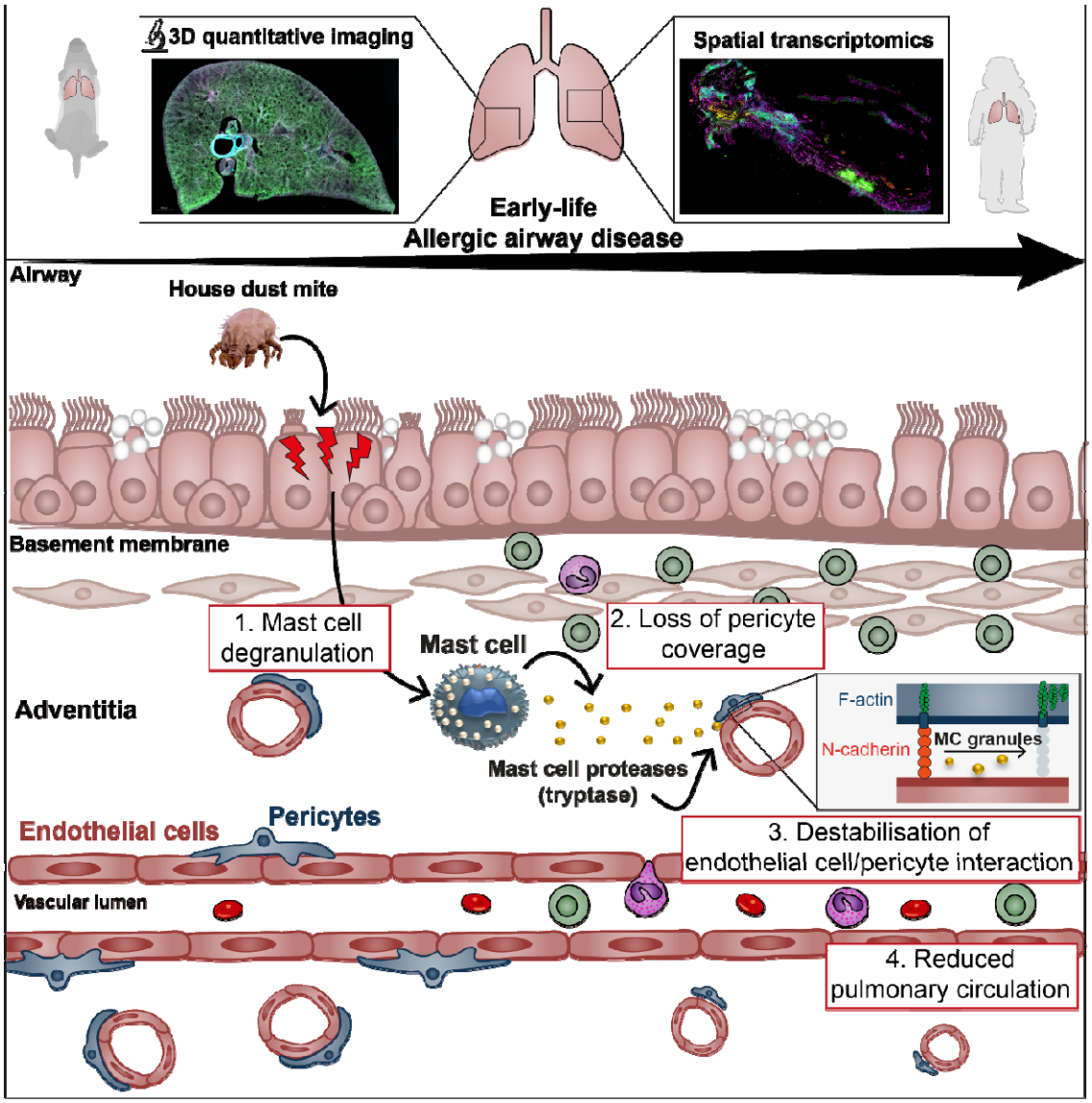

Figure 8: Graphical abstract. MC degranulation during early life allergic airway disease leads to pericyte damage and associated vascular remodelling in the lung adventitia.

References

Allakhverdi, Z., Smith, D.E., Comeau, M.R., and Delespesse, G. (2007). Cutting edge: The ST2 ligand IL-33 potently activates and drives maturation of human mast cells. Journal of immunology (Baltimore, Md : 1950) *179*, 2051-2054.

Armulik, A., Genove, G., and Betsholtz, C. (2011). Pericytes: developmental, physiological, and pathological perspectives, problems, and promises. Developmental cell *21*, 193-215.

Armulik, A., Genove, G., Mae, M., Nisancioglu, M.H., Wallgard, E., Niaudet, C., He, L., Norlin, J., Lindblom, P., Strittmatter, K.*, et al.* (2010). Pericytes regulate the blood-brain barrier. Nature *468*, 557-561.

Attwell, D., Mishra, A., Hall, C.N., O'Farrell, F.M., and Dalkara, T. (2016). What is a pericyte? J Cereb Blood Flow Metab *36*, 451-455.

Augusto, L.S., Silva, G.C., Pinho, J.F., Aires, R.D., Lemos, V.S., Ramalho, L.F.C., Jentzsch, N.S., and Rodrigues-Machado, M.G. (2017). Vascular function in asthmatic children and adolescents. Respiratory Research *18*, 17.

Barkaway, A., Attwell, D., and Korte, N. (2022). Immune–vascular mural cell interactions: consequences for immune cell trafficking, cerebral blood flow, and the blood–brain barrier. *9 %J Neurophotonics*, 031914.

Bordenave, J., Tu, L., Berrebeh, N., Thuillet, R., Cumont, A., Le Vely, B., Fadel, E., Nadaud, S., Savale, L., Humbert, M.*, et al.* (2020). Lineage Tracing Reveals the Dynamic Contribution of Pericytes to the Blood Vessel Remodeling in Pulmonary Hypertension. Arterioscler Thromb Vasc Biol *40*, 766-782.

Bradding, P., and Arthur, G. (2016). Mast cells in asthma--state of the art. Clinical and experimental allergy : journal of the British Society for Allergy and Clinical Immunology *46*, 194-263.

Burgstaller, G., Vierkotten, S., Lindner, M., Konigshoff, M., and Eickelberg, O. (2015). Multidimensional immunolabeling and 4D time-lapse imaging of vital ex vivo lung tissue. Am J Physiol Lung Cell Mol Physiol *309*, L323-332.

Castanhinha, S., Sherburn, R., Walker, S., Gupta, A., Bossley, C.J., Buckley, J., Ullmann, N., Grychtol, R., Campbell, G., Maglione, M.*, et al.* (2015). Pediatric severe

asthma with fungal sensitization is mediated by steroid-resistant IL-33. J Allergy Clin Immunol *136*, 312-322 e317.

Cautivo, K.M., Matatia, P.R., Lizama, C.O., Mroz, N.M., Dahlgren, M.W., Yu, X., Sbierski-Kind, J., Taruselli, M.T., Brooks, J.F., Wade-Vallance, A.*, et al.* (2022). Interferon gamma constrains type 2 lymphocyte niche boundaries during mixed inflammation. Immunity *55*, 254-271 e257.

Cautivo, K.M., Steer, C.A., and Molofsky, A.B. (2020). Immune outposts in the adventitia: One foot in sea and one on shore. Curr Opin Immunol *64*, 34-41.

Cheng, L.E., Hartmann, K., Roers, A., Krummel, M.F., and Locksley, R.M. (2013). Perivascular mast cells dynamically probe cutaneous blood vessels to capture immunoglobulin E. Immunity *38*, 166-175.

Choi, H.W., Suwanpradid, J., Kim, I.H., Staats, H.F., Haniffa, M., MacLeod, A.S., and Abraham, S.N. (2018). Perivascular dendritic cells elicit anaphylaxis by relaying allergens to mast cells via microvesicles. Science (New York, NY) *362*.

Dahlgren, M.W., Jones, S.W., Cautivo, K.M., Dubinin, A., Ortiz-Carpena, J.F., Farhat, S., Yu, K.S., Lee, K., Wang, C., Molofsky, A.V.*, et al.* (2019). Adventitial Stromal Cells Define Group 2 Innate Lymphoid Cell Tissue Niches. Immunity *50*, 707-722 e706.

de Kleer, I.M., Kool, M., de Bruijn, M.J., Willart, M., van Moorleghem, J., Schuijs, M.J., Plantinga, M., Beyaert, R., Hams, E., Fallon, P.G.*, et al.* (2016). Perinatal Activation of the Interleukin-33 Pathway Promotes Type 2 Immunity in the Developing Lung. Immunity *45*, 1285-1298.

Deprez, M., Zaragosi, L.E., Truchi, M., Becavin, C., Ruiz Garcia, S., Arguel, M.J., Plaisant, M., Magnone, V., Lebrigand, K., Abelanet, S.*, et al.* (2020). A Single-Cell Atlas of the Human Healthy Airways. American journal of respiratory and critical care medicine *202*, 1636-1645.

Derakhshan, T., Samuchiwal, S.K., Hallen, N., Bankova, L.G., Boyce, J.A., Barrett, N.A., Austen, K.F., and Dwyer, D.F. (2021). Lineage-specific regulation of inducible and constitutive mast cells in allergic airway inflammation. The Journal of experimental medicine *218*.

Dharmage, S.C., Perret, J.L., and Custovic, A. (2019). Epidemiology of Asthma in Children and Adults. Frontiers in pediatrics *7*, 246.

Dudeck, J., Froebel, J., Kotrba, J., Lehmann, C.H.K., Dudziak, D., Speier, S., Nedospasov, S.A., Schraven, B., and Dudeck, A. (2019). Engulfment of mast cell secretory granules on skin inflammation boosts dendritic cell migration and priming efficiency. J Allergy Clin Immunol *143*, 1849-1864.e1844.

Dudeck, J., Kotrba, J., Immler, R., Hoffmann, A., Voss, M., Alexaki, V.I., Morton, L., Jahn, S.R., Katsoulis-Dimitriou, K., Winzer, S.*, et al.* (2021). Directional mast cell degranulation of tumor necrosis factor into blood vessels primes neutrophil extravasation. Immunity *54*, 468-483 e465.

Erdener Ş, E., Küreli, G., and Dalkara, T. (2022). Contractile apparatus in CNS capillary pericytes. Neurophotonics *9*, 021904.

Gaudenzio, N., Sibilano, R., Marichal, T., Starkl, P., Reber, L.L., Cenac, N., McNeil, B.D., Dong, X., Hernandez, J.D., Sagi-Eisenberg, R.*, et al.* (2016). Different activation signals induce distinct mast cell degranulation strategies. The Journal of clinical investigation *126*, 3981-3998.

Girbl, T., Lenn, T., Perez, L., Rolas, L., Barkaway, A., Thiriot, A., Del Fresno, C., Lynam, E., Hub, E., Thelen, M.*, et al.* (2018). Distinct Compartmentalization of the Chemokines CXCL1 and CXCL2 and the Atypical Receptor ACKR1 Determine Discrete Stages of Neutrophil Diapedesis. Immunity *49*, 1062-1076 e1066.

Gregory, L.G., Causton, B., Murdoch, J.R., Mathie, S.A., O'Donnell, V., Thomas, C.P., Priest, F.M., Quint, D.J., and Lloyd, C.M. (2009). Inhaled house dust mite induces pulmonary T helper 2 cytokine production. Clinical and experimental allergy : journal of the British Society for Allergy and Clinical Immunology *39*, 1597-1610.

Hammad, H., and Lambrecht, B.N. (2021). The basic immunology of asthma. Cell *184*, 2521-2522.

Harkness, L.M., Ashton, A.W., and Burgess, J.K. (2015). Asthma is not only an airway disease, but also a vascular disease. Pharmacology & Therapeutics *148*, 17-33.

He, S., Gaca, M.D., and Walls, A.F. (1998). A role for tryptase in the activation of human mast cells: modulation of histamine release by tryptase and inhibitors of tryptase. The Journal of pharmacology and experimental therapeutics *286*, 289-297.

Hung, C.F., Wilson, C.L., Chow, Y.H., Liles, W.C., Gharib, S.A., Altemeier, W.A., and Schnapp, L.M. (2022). Effect of lung pericyte-like cell ablation on the bleomycin model of injury and repair. Am J Physiol Lung Cell Mol Physiol *322*, L607-L616.

Hung, C.F., Wilson, C.L., and Schnapp, L.M. (2019). Pericytes in the Lung. Advances in experimental medicine and biology *1122*, 41-58.

Johnson, J.R., Folestad, E., Rowley, J.E., Noll, E.M., Walker, S.A., Lloyd, C.M., Rankin, S.M., Pietras, K., Eriksson, U., and Fuxe, J. (2015). Pericytes contribute to airway remodeling in a mouse model of chronic allergic asthma. Am J Physiol Lung Cell Mol Physiol *308*, L658-671.

Joulia, R., Gaudenzio, N., Rodrigues, M., Lopez, J., Blanchard, N., Valitutti, S., and Espinosa, E. (2015). Mast cells form antibody-dependent degranulatory synapse for dedicated secretion and defence. Nat Commun *6*, 6174.

Joulia, R., Guerrero-Fonseca, I.M., Girbl, T., Coates, J.A., Stein, M., Vázquez-Martínez, L., Lynam, E., Whiteford, J., Schnoor, M., Voehringer, D*., et al.* (2022). Neutrophil breaching of the blood vessel pericyte layer during diapedesis requires mast cell-derived IL-17A. Nature Communications *13*, 7029.

Joulia, R., L'Faqihi, F.E., Valitutti, S., and Espinosa, E. (2017). IL-33 fine tunes mast cell degranulation and chemokine production at the single-cell level. J Allergy Clin Immunol *140*, 497-509 e410.

Kruse, K., Lee, Q.S., Sun, Y., Klomp, J., Yang, X., Huang, F., Sun, M.Y., Zhao, S., Hong, Z., Vogel, S.M*., et al.* (2018). N-cadherin signaling via Trio assembles adherens junctions to restrict endothelial permeability. Journal of Cell Biology *218*, 299-316.

Kunder, C.A., St John, A.L., and Abraham, S.N. (2011). Mast cell modulation of the vascular and lymphatic endothelium. Blood *118*, 5383-5393.

Kureli, G., Yilmaz-Ozcan, S., Erdener, S.E., Donmez-Demir, B., Yemisci, M., Karatas, H., and Dalkara, T. (2020). F-actin polymerization contributes to pericyte contractility in retinal capillaries. Experimental neurology *332*, 113392.

Lloyd, C.M., and Saglani, S. (2019). Opening the Window of Immune Opportunity: Treating Childhood Asthma. Trends Immunol *40*, 786-798.

Madissoon, E., Oliver, A.J., Kleshchevnikov, V., Wilbrey-Clark, A., Polanski, K., Richoz, N., Ribeiro Orsi, A., Mamanova, L., Bolt, L., Elmentaite, R*., et al.* (2022). A

spatially resolved atlas of the human lung characterizes a gland-associated immune niche. Nat Genet.

McDonald, D.M. (2001). Angiogenesis and remodeling of airway vasculature in chronic inflammation. American journal of respiratory and critical care medicine *164*, S39-45.

Mukherjee, M., Stoddart, A., Gupta, R.P., Nwaru, B.I., Farr, A., Heaven, M., Fitzsimmons, D., Bandyopadhyay, A., Aftab, C., Simpson, C.R.*, et al.* (2016). The epidemiology, healthcare and societal burden and costs of asthma in the UK and its member nations: analyses of standalone and linked national databases. BMC medicine *14*, 113.

Nikolakopoulou, A.M., Montagne, A., Kisler, K., Dai, Z., Wang, Y., Huuskonen, M.T., Sagare, A.P., Lazic, D., Sweeney, M.D., Kong, P.*, et al.* (2019). Pericyte loss leads to circulatory failure and pleiotrophin depletion causing neuron loss. Nature neuroscience *22*, 1089-1098.

Nortley, R., Korte, N., Izquierdo, P., Hirunpattarasilp, C., Mishra, A., Jaunmuktane, Z., Kyrargyri, V., Pfeiffer, T., Khennouf, L., Madry, C.*, et al.* (2019). Amyloid beta oligomers constrict human capillaries in Alzheimer's disease via signaling to pericytes. Science (New York, NY) *365*.

Papi, A., Brightling, C., Pedersen, S.E., and Reddel, H.K. (2018). Asthma. Lancet *391*, 783-800.

Pejler, G. (2019). The emerging role of mast cell proteases in asthma. The European respiratory journal *54*, 1900685.

Pejler, G., Ronnberg, E., Waern, I., and Wernersson, S. (2010). Mast cell proteases: multifaceted regulators of inflammatory disease. Blood *115*, 4981-4990.

Procter, T.V., Williams, A., and Montagne, A. (2021). Interplay between Brain Pericytes and Endothelial Cells in Dementia. Am J Pathol *191*, 1917-1931.

Puttur, F., Denney, L., Gregory, L.G., Vuononvirta, J., Oliver, R., Entwistle, L.J., Walker, S.A., Headley, M.B., McGhee, E.J., Pease, J.E.*, et al.* (2019). Pulmonary environmental cues drive group 2 innate lymphoid cell dynamics in mice and humans. Sci Immunol *4*.

Rowley, J.E., and Johnson, J.R. (2014). Pericytes in chronic lung disease. International archives of allergy and immunology *164*, 178-188.

Roy, A., Sawesi, O., Pettersson, U., Dagalv, A., Kjellen, L., Lunden, A., and Abrink, M. (2016). Serglycin proteoglycans limit enteropathy in Trichinella spiralis-infected mice. BMC Immunol *17*, 15.

Saglani, S., Gregory, L.G., Manghera, A.K., Branchett, W.J., Uwadiae, F., Entwistle, L.J., Oliver, R.A., Vasiliou, J.E., Sherburn, R., Lui, S.*, et al.* (2018). Inception of early-life allergen-induced airway hyperresponsiveness is reliant on IL-13(+)CD4(+) T cells. Sci Immunol *3*.

Saglani, S., Lui, S., Ullmann, N., Campbell, G.A., Sherburn, R.T., Mathie, S.A., Denney, L., Bossley, C.J., Oates, T., Walker, S.A.*, et al.* (2013). IL-33 promotes airway remodeling in pediatric patients with severe steroid-resistant asthma. Journal of Allergy and Clinical Immunology *132*, 676-685.e613.

Saluzzo, S., Gorki, A.D., Rana, B.M.J., Martins, R., Scanlon, S., Starkl, P., Lakovits, K., Hladik, A., Korosec, A., Sharif, O.*, et al.* (2017). First-Breath-Induced Type 2 Pathways Shape the Lung Immune Environment. Cell reports *18*, 1893-1905.

Salvato, G. (2001). Quantitative and morphological analysis of the vascular bed in bronchial biopsy specimens from asthmatic and non-asthmatic subjects. Thorax *56*, 902-906.

Schupp, J.C., Adams, T.S., Cosme, C., Jr., Raredon, M.S.B., Yuan, Y., Omote, N., Poli, S., Chioccioli, M., Rose, K.A., Manning, E.P.*, et al.* (2021a). Integrated Single-Cell Atlas of Endothelial Cells of the Human Lung. Circulation *144*, 286-302.

Schupp, J.C., Adams, T.S., Cosme, C., Raredon, M.S.B., Yuan, Y., Omote, N., Poli, S., Chioccioli, M., Rose, K.-A., Manning, E.P.*, et al.* (2021b). Integrated Single-Cell Atlas of Endothelial Cells of the Human Lung. *144*, 286-302.

Stenmark, K.R., Nozik-Grayck, E., Gerasimovskaya, E., Anwar, A., Li, M., Riddle, S., and Frid, M. (2011). The Adventitia: Essential Role in Pulmonary Vascular Remodeling. In Comprehensive Physiology, pp. 141-161.

Turato, G., Barbato, A., Baraldo, S., Zanin, M.E., Bazzan, E., Lokar-Oliani, K., Calabrese, F., Panizzolo, C., Snijders, D., Maestrelli, P.*, et al.* (2008). Nonatopic children with multitrigger wheezing have airway pathology comparable to atopic asthma. American journal of respiratory and critical care medicine *178*, 476-482.

Turner, D.L., Goldklang, M., Cvetkovski, F., Paik, D., Trischler, J., Barahona, J., Cao, M., Dave, R., Tanna, N., D'Armiento, J.M.*, et al.* (2018). Biased Generation and In

Situ Activation of Lung Tissue-Resident Memory CD4 T Cells in the Pathogenesis of Allergic Asthma. Journal of immunology (Baltimore, Md : 1950) *200*, 1561-1569.

Xing, W., Austen, K.F., Gurish, M.F., and Jones, T.G. (2011). Protease phenotype of constitutive connective tissue and of induced mucosal mast cells in mice is regulated by the tissue. Proceedings of the National Academy of Sciences of the United States of America *108*, 14210-14215.

Yuan, K., Agarwal, S., Chakraborty, A., Condon, D.F., Patel, H., Zhang, S., Huang, F., Mello, S.A., Kirk, O.I., Vasquez, R.*, et al.* (2021). Lung Pericytes in Pulmonary Vascular Physiology and Pathophysiology. Comprehensive Physiology *11*, 2227-2247.

Zimmerman, S.M., Fropf, R., Kulasekara, B.R., Griswold, M., Appelbe, O., Bahrami, A., Boykin, R., Buhr, D.L., Fuhrman, K., Hoang, M.L.*, et al.* (2022). Spatially resolved whole transcriptome profiling in human and mouse tissue using Digital Spatial Profiling. 2021.2009.2029.462442.

Acknowledgments

This work was supported by funds from the Wellcome Trust (107059/Z/15/Z and 220254/Z/20/Z) to C.M.L. R.J. is supported by fellowships from the British Heart Foundation Imperial College Centre for Research Excellence (RE/18/4/34215). The Facility for Imaging by Light Microscopy (FILM) at Imperial College London is part-supported by funding from the Wellcome Trust (grant 104931/Z/14/Z) and the authors would like to thank Dr. David Gaboriau for invaluable help.

Author contributions

Conceptualization, R.J., F.P., C.M.L. Methodology, R.J., F.P. Investigation, R.J., F.P., H.S., A.V., L.J.E., Resources, M.A., K.B., E.S., P.M., R.J.H., S.A.W., L.Y., S.S. Formal analysis, R.J., F.P. and A.V. Visualization, R.J. Writing – original draft. R.J. Writing – review & editing, R.J., F.P., H.S., A.V., L.J.E., M.A., K.B., E.S., P.M., R.J.H., S.A.W., L.Y., S.S. and C.M.L. Supervision, R.J. and C.M.L.

Declaration of interests

The authors declare no competing interests. L.J.E. is now an employee of GSK however GSK did not contribute to any of the work in this study.

STAR Methods

Resource availability

Lead contact

Further information and requests for resources and reagents should be directed to and will be fulfilled by lead author Régis Joulia (r.joulia@imperial.ac.uk)

Materials availability

This study did not generate new unique reagents.

Experimental model and subject details

Animals and reagents: WT BALB/c (stock number #000651) were initially obtained from Charles River (UK) and maintained by in-house breeding. Each mother with its litter was housed separately. Mice were maintained in specific pathogen–free conditions and given food and water ad libitum. In individual experiments, all mice were matched for age and background strain. All in vivo experiments were conducted at the NHLI, Imperial College London, UK under the UK legislation for animal experimentation (PPL P996A24E1 and PP8328343) and in agreement with the UK Home Office Animals Scientific Procedures Act 1986 (ASPA).

Randomization: Neonatal mice were of either sex, and litters were randomly assigned to control or experimental groups.

Sample size: The number of mice analysed for each different experimental approach is indicated on each figure.

Human donors: Demographic and clinical information can be found in Table S1. Human adult samples used in this research project were obtained from the Imperial

College Healthcare Tissue Bank (ICHTB). ICHTB is supported by the National Institute for Health Research (NIHR) Biomedical Research Centre based at Imperial College Healthcare NHS Trust and Imperial College London. ICHTB is approved by Wales REC3 to release human material for research (17/WA/0161), and the samples for this project (R22006) were issued from sub-collection reference number ICB_NC_21_017. The views expressed are those of the author(s) and not necessarily those of the NHS, the NIHR or the Department of Health.

School aged children (aged 9-17) that were undergoing a clinically indicated bronchoscopy, were recruited. Donor clinical data are available in Table S1. The study was approved by the institutional ethics committee, and written, informed parental consent and child assent were obtained.

Neonatal AAD: Neonatal mice were exposed repeatedly to either HDM (Greer Lot#360923) or PBS, intranasally from PN d. During the first 2 weeks of life, mice were administered 10 µg of HDM extract in 10 µl of PBS, three times a week. From week 3, mice received 15 µg of HDM in 15 µl of PBS. All outputs were assessed at 24 hours after allergen challenge (Gregory et al., 2009).

Precision-cut lung slices (PCLS): PCLSs provided a 3D cell culture model to image vascular remodelling within the lung microenvironment and was adapted from previously described protocols (Burgstaller et al., 2015; Puttur et al., 2019).

For mouse PLCS, lungs were inflated *in situ* with 0.4 ml of 2% low-melting agarose (Thermo Fisher Scientific) in PBS. After inflation, lungs were carefully dissected out and fixed in 4% Paraformaldehyde (PFA, Electron Microscopy Sciences) overnight at 4° C. Human lung tissue was collected from anonymised donors at Hammersmith and Royal Brompton hospitals NHS trusts and immediately fixed in 4% PFA

overnight at 4ºC. Following fixation, 100-200 µm transverse sections were prepared using a Compresstome VF-300 vibrating microtome (Precisionary Instruments).

PCLS were permeabilised in PBS complemented with 0.5% Triton (Sigma) for 1 hour at room temperature then blocked in animal-free blocker (2BSCIENTIFIC LTD) for 1 hour. Slices were incubated with indicated primary antibodies overnight at 4º C in 25% animal free blocker in PBS, and where required PCLS were incubated with secondary antibodies for 5 hours at room temperature in 25% animal free blocker in PBS. Lungs slices were mounted on microscopic slides (ThermoFisher) and immerged in ProLong Diamond (ThermoFisher) and kept at 4º C until image acquisition.

Image acquisition: Images were acquired on a LEICA SP4 or SP8 (LEICA) using 20X objective (NA 0.7 and 0.75 for SP4 and SP8 respectively) or 10X objective (NA 0.4 for SP4 and SP8) with a resolution of 512x512 or 1024x1024 pixels. Motorised stages of the microscopes were employed for tile scan imaging and merged using LEICA built-in software (LAS) with a 10% overlap threshold. Adventitial regions (bronchovascular region) were defined as a lung region with the presence of a large airway (i.e. distinct stratified epithelium) and intermediate/large blood vessel. Vasculature associated to adventitial region was analysed within a 150 µm radius from the main airway/large vessel. Parenchymal regions were identified morphologically based on the alveoli structure more than 300 µm from any large airways.

Image analysis: Image analysis and rendering were performed using IMARIS 8.1 or 9.3 (Bitplane). LIF files were converted into IMARIS .ims files using IMARIS Converter software v9.9.1 (Bitplane). Cell and HIF-1α spot number was analysed

using the semi-automatic spot function (cell diameter 10 and 15 µm for leukocytes and pericytes respectively) and volumes (i.e. EC/pericyte coverage) were determined using the surface function. Numbers of cells were normalised to the total volume of the image. Thresholds for cell volume analysis in PCLS sections were maintained across the experimental conditions to provide accurate comparisons. Pericyte and endothelial cell volumes were determined using the cell function of IMARIS and similar thresholds for cell cytoplasm were used across all the experimental conditions using either CMTMR staining or F-actin. All image analysis was performed on raw images without fluorescence modification. Fiji (imageJ) functions (i.e. 3D surface plot and line measurement) were used to perform colocalization analysis.

Cell purification: Lung tissues were gently dissociated in small fragments (1-5 mm length) using scissors then placed in 6 wells plates (Corning). To generate pericytes, mouse and human lung samples were differentiated as previously described with small modifications (Girbl et al., 2018). Briefly, cells were grown in Dulbecco's Modified Eagle's Medium (DMEM) supplemented with 10% FCS, 100 U/mL penicillin, 100 mg/mL streptomycin (all Thermo Fisher Scientific) and 100 pM pigment epithelium-derived factor (PEDF, Sigma-Aldrich). After 15 to 22 days of culture, cells were detached using trypsin (Thermo Fisher) and isolated using the EasySep™ APC Positive Selection Kit II (StemCell) according to manufacturer instructions. APC conjugated anti-PDGFRβ was used for magnetic cell sorting. Cell purity (PDGFRβ^{+}NG2^{-}) was assessed by flow cytometry.

Mouse lung MCs were grown in OPTI-MEM supplemented with 10% FCS, 100 U/mL penicillin, 100 mg/mL streptomycin and 4% CHO transfectants secreting murine Stem Cell Factor (SCF, a gift from Dr P. Dubreuil, Marseille, France, 4% correspond

to ~50 ng/ml SCF) for 6-8 weeks. Human lung MCs were grown in OPTI-MEM supplemented with 2.5% BSA, 100 U/mL penicillin, 100 mg/mL streptomycin and 4% CHO transfectants secreting murine SCF for ~8 weeks. Mast cell purity was assessed by flow cytometry ($CD117^+/Fc\varepsilon RI^+$).

Functional assays: Mouse or human pericytes (~10,000 cells) were seeded onto µ-Slide 8 Well high ibiTreat: tissue culture treated (Ibidi) and leave to rest for 24 hours. Cells were stained using CellTracker™ Orange CMTMR Dye (ThermoFisher) according to manufacture instructions. ~5,000 previously anti-dinitrophenyl (DNP) IgE-sensitized lung MCs (overnight at 1 µg/ml, clone SPE-7, Merck) were washed in Tyrode buffer (Merck) and placed on top of pericytes for ~15 minutes at 37° C. Increasing concentrations of DNP-BSA (Merck) were added and cells were left for 24 hours at 37° C. In some experiments, protease inhibitor cocktail (Merck) was used according to manufacturer instructions or pericytes were directly exposed to recombinant m-MCP6 (R&D systems, matured according to manufacturer instructions) or 10 µM of APC-366 (tryptase inhibitor, Merck) was employed to block human tryptase. Following incubation, cells were placed on ice and stained for surface markers for 30 minutes, washed and fixed for ~15 minutes with 4% PFA at 37° C. Where necessary, fixed cells were permeabilised using Permeabilization Buffer (ThermoFisher) and stained for 30 minutes at room temperature with fluorochrome-conjugated antibodies or for F-actin (Alexa Fluor™ 488 Phalloidin, ThermoFisher). Cells were kept in PBS before image acquisition. Mast cell degranulation flow cytometry assay were performed as previously described (Joulia et al., 2015). Briefly, ~10000 IgE sensitized lung MCs were washed in Tyrode buffer (Merck) and placed in a 96 wells U bottom plates at 37°C. Cells were stimulated with

increasing DNP-BSA concentrations (Merck) for 30 minutes at 37°C, collected and processed for flow cytometry.

Flow cytometry: Cells were resuspended and washed in PBS + 0.5% BSA + 0.1 mM EDTA. Primary antibodies were incubated for ~30 minutes at 4° C, washed 2 times and incubated with secondary antibodies if necessary for another 30 minutes at 4° C. Data were acquired on a BD LSR Fortessa using FACSDIVA software (both from BD Biosciences) and analysed using FlowJo software (v10, FlowJo).

scRNAseq analysis: Mouse and human pericyte marker analysis was performed using the publicly available data mining website (http://lungendothelialcellatlas.com/) (Schupp et al., 2021a). Data were visualised using the multi-gene query options and the expression of the best 8 markers for pericytes were analysed in mouse and human scRNAseq datasets (30000 cells combined from 5 cohorts).

Spatial transcriptomics: We followed experimental methods (NanoString) described in the publication (Zimmerman et al., 2022). Briefly, FFPE human lung samples were baked overnight at 37° C followed by 3 hours of baking at 65° C, then loaded onto a Leica Bond RX Fully Automated Research Stainer for subsequent processing steps. The processing protocol included three major steps: 1) slide baking, 2) antigen retrieval for 20 min at 100° C, and 3) treatment with Proteinase K (1.0 µg/mL in 1xPBS) for 15 min. Following these steps, slides were removed from the Leica Bond RX, and a cocktail of GeoMx Cancer Transcriptome Atlas probes (specific to ~1,800 genes separate targets) were applied to each slide and allowed to hybridize at 37° C overnight in a humidity chamber. The following day, slides were washed, blocked, and allowed to incubate with a combination of Alexa Fluor 488-labeled anti-alpha smooth muscle actin antibody (Invitrogen/Thermo product #: 53-9760-82; clone:

1A4), Alexa Fluor 594-labeled Anti-vimentin antibody (Santa Cruz product #: sc-373717 AF594; clone: E-5), Alexa Fluor 647-labeled anti-CD45 antibody (Cell Signaling Technology product #: 13917BF; clone: D9M8I), and Syto83 nucleic acid stain. Slides were stained for 1 h at room temperature in a humidity chamber. Slides were then washed and loaded onto a GeoMx instrument. On the GeoMx machine, slides were fluorescently scanned, and ROIs were collected from the following areas: smooth muscle, epithelium, fibroblast (vessel-rich), and immune-rich. The GeoMx device exposed ROIs to 385 nm light (UV), releasing the indexing oligos. Indexing oligos were collected with a microcapillary and deposited into a 96-well plate. Samples were dried down overnight, then resuspended in 10 µL of DEPC-treated water. PCR was performed using 4 µL of each sample and the oligos from each ROI were indexed using unique i5 and i7 dual-indexing systems (Illumina). PCR reactions were purified twice using AMPure XP beads (Beckman Coulter, Inc) according to the manufacturer's protocol. Purified libraries were sequenced on an Illumina NovaSeq 6000. Data analysis was performed as described (Zimmerman et al., 2022). Following removal of targets consistently below the limit of quantification (i.e. <5000 raw reads) and negative probes, the limit of detection above which a gene was called "detected" was defined as 2 standard deviations above the geometric mean of negative probes. Datasets were normalized using upper quartile (Q3) normalization. Data for cell deconvolution were obtained from Deprez et al. (Deprez et al., 2020). Data analysis was then performed using the DSP platform. PCA, pathway analysis (GSEA) and volcano plots analysis were performed on the DSP platform and data were extracted and represented using Prism software. Spatial expression of gene of interest was performed using the DSP platform, the expression of the gene (counts) is indicated by the areas of the bubbles normalised across all the ROIs.

Statistical analysis: Most statistical analyses including PCA were performed using Prism software (GraphPad v9.4.1). For the Volcano plots, significance levels were defined as p value <0.05 (Mann-Whitney t test) and genes exhibiting more than 0.5 log2 expression difference between the 2 regions analysed. t-SNE analysis was performed using build-in functions of FlowJo software, iterations were fixed at 1000, perplexity 30 and learning rate 22. The results are expressed as means ± SEM and the n numbers for each dataset are provided in the Figure legends. Comparisons between two groups were carried out using the paired or unpaired Student's or Mann-Whitney t test as appropriate. One-way ANOVA followed by Tukey post hoc test was performed for multiple group comparisons. Statistical significance was accepted at $p < 0.05$.

Data and Code availability

Any additional information required to reanalyse the data reported in this paper is available from the lead contact upon request. Original single cell spatial transcriptomic data are available as supplementary data attached to this paper. The paper does not report original code.